

Traction and strain-rate at the base of the lithosphere: an insight into cratonic survival

Jyotirmoy Paul ¹, Attreyee Ghosh ¹ and Clinton P. Conrad ²

¹Centre for Earth Sciences, Indian Institute of Science, Bangalore 560012, India. E-mail: jyotirmoy@iisc.ac.in

²Centre for Earth Evolution and Dynamics (CEED), University of Oslo, N-0315 Oslo, Norway

Accepted 2019 February 5. Received 2019 February 1; in original form 2018 November 10

SUMMARY

Cratons are the oldest parts of the lithosphere, some of them surviving since Archean. Their long-term survival has sometimes been attributed to high viscosity and low density. In our study, we use a numerical model to examine how shear tractions exerted by mantle convection work to deform cratons by convective shearing. We find that although tractions at the base of the lithosphere increase with increasing lithosphere thickness, the associated strain-rates decrease. This inverse relationship between stress and strain-rate results from lateral viscosity variations along with the model's free-slip condition imposed at the Earth's surface, which enables strain to accumulate along weak zones at plate boundaries. Additionally, we show that resistance to lithosphere deformation by means of convective shearing, which we express as an apparent viscosity, scales with the square of lithosphere thickness. This suggests that the enhanced thickness of the cratons protects them from convective shear and allows them to survive as the least deformed areas of the lithosphere. Indeed, we show that the combination of a smaller asthenospheric viscosity drop and a larger cratonic viscosity, together with the excess thickness of cratons compared to the surrounding lithosphere, can explain their survival since Archean time.

Key words: Mantle processes; Numerical modelling; Cratons; Dynamics of lithosphere and mantle.

1 INTRODUCTION

Cratons are the missing links in Earth's long history of geodynamic evolution. In addition to their significant age, cratons generally have a thick and cold lithosphere (Jordan 1975, 1978; Polet & Anderson 1995; Rudnick *et al.* 1998; Lenardic & Moresi 1999; Artemieva & Mooney 2002; Gung *et al.* 2003; Lenardic *et al.* 2003; King 2005; Cooper *et al.* 2006). Their endurance provokes a fundamental question about the special conditions that have protected them from the destructive forces of mantle dynamics, providing a longer survival time than any other type of lithosphere, for example, oceanic or non-cratonic continental lithosphere (Lenardic & Moresi 1999; Shapiro *et al.* 1999; Lenardic *et al.* 2000, 2003; Sleep 2003; King 2005; Cooper *et al.* 2006; O'Neill *et al.* 2008; Yoshida 2010, 2012; Wang *et al.* 2014). The craton stabilization ages determined by rhenium depletion peak around 3 Ga (Pearson *et al.* 1995a,b; Pearson & Wittig 2014). This age is marked by several important geophysical and geochemical phenomena that may have resulted in a global change of the Earth's geodynamics, possibly by initiation of plate tectonics (Sizova *et al.* 2015; Hawkesworth *et al.* 2016; Tang *et al.* 2016;

Hawkesworth *et al.* 2017). By this time, mantle had cooled down sufficiently (Moore & Webb 2013; Sizova *et al.* 2015; Hawkesworth *et al.* 2017) and significant changes in the composition of continental crust, from mafic to intermediate (Tang *et al.* 2016), had taken place. These changes might have provided an opportunity to form low density and high viscosity, thick continental lithosphere (Beall *et al.* 2018), which could be the reason for craton stabilization at that time.

Early studies (Jordan 1975, 1978; Lenardic & Moresi 1999; Lenardic *et al.* 2003) advocated that the compositional buoyancy and high viscosity of thick cratons may be responsible for their long-term survival. In his Tectosphere hypothesis, Jordan (1975) proposed that the cratons, equipped with compositional buoyancy, are capable of surviving convective recycling. However, in numerical models, cratons with low density, high viscosity and high yield strength experienced a much longer survival time than those with only chemically buoyant roots (Lenardic & Moresi 1999; Lenardic *et al.* 2003). Wang *et al.* (2014) have proposed compositional density as a secondary factor for their survival, with compositional rheology (e.g. viscosity) being primary. Recent studies have shown

that a part of the North American craton is deforming at a faster rate because of its low compositional density (Kaban *et al.* 2015). Thus, it is likely that the viscosity of cratons plays a more significant role in cratonic survival than does craton density. The long-term survival of high viscosity cratons has been studied numerically before (Lenardic & Moresi 1999; Lenardic *et al.* 2000, 2003; O'Neill *et al.* 2008; Yoshida 2010, 2012; Wang *et al.* 2014); however, estimates of the appropriate viscosity for cratons remain controversial.

In this study, we use numerical models of global mantle flow to understand how shear tractions at the base of the lithosphere play a role in the deformation of cratons. We relate these tractions to strain-rates, which indicate how cratons are deforming due to the convective shear within the mantle. Our analysis builds upon work by Conrad & Lithgow-Bertelloni (2006), who employed no-slip boundary conditions at the surface and showed that traction magnitudes increase with increasing thickness of the lithosphere. Cooper & Conrad (2009), using an analytical model of constant viscosity at the base of the lithosphere, showed that these tractions cause sublithospheric strain-rates to increase exponentially as the lithosphere thickness increases, thus potentially limiting the maximum thickness of cratons. However, the actual surface of the Earth is a free-slip condition, meaning that the lithosphere can move laterally in response to basal tractions instead of deforming locally beneath a rigid surface. This plate tectonic response of the lithosphere should affect the relationship between basal tractions and deformation, and thus our interpretation of craton survival time as well. Additionally, lateral viscosity variations (LVV) could also significantly influence the strain-rate patterns at the base of the lithosphere. In our study, we use instantaneous 3-D global mantle convection models to examine how cratonic viscosity structure and thickness relate to strain-rates beneath the cratons. We assume present-day craton locations from the lithospheric thickness model of Conrad & Lithgow-Bertelloni (2006). From our results, we attempt to estimate a critical viscosity structure for cratons that can explain their survival above the Earth's dynamically convecting mantle.

Interpreting the viscosity structure of cratons is the key to understanding their long-term survival. Several studies have shown that there is a significant viscosity contrast between cratonic and non-cratonic lithosphere. The estimated viscosity contrast calculated by Lenardic *et al.* (2003) was 1000 times whereas O'Neill *et al.* (2008) estimated a viscosity contrast of 50–150 times between cratons and their surroundings. In another study, using 2-D box model, Wang *et al.* (2014) had shown that a very small viscosity contrast (of the order of 10) can protect the cratons if non-Newtonian flow laws are considered. These studies are more focused on the local dynamics (mechanics of dripping, rifting or other destabilization mechanisms) rather than the overall relation between thickness, viscosity and survival potential. Instead, our main focus is to measure the shear strain-rates under cratons and not their gravitational instability above a convecting mantle.

2 METHODS

2.1 Mantle flow

We develop instantaneous models of global mantle flow using CitcomS (Zhong *et al.* 2000), a finite element code that solves the thermochemical convection equations in an anelastic, viscous and incompressible spherical shell. The code solves the governing equations for thermal convection, considering conservation of mass, momentum and energy, assuming Boussinesq approximation. We have

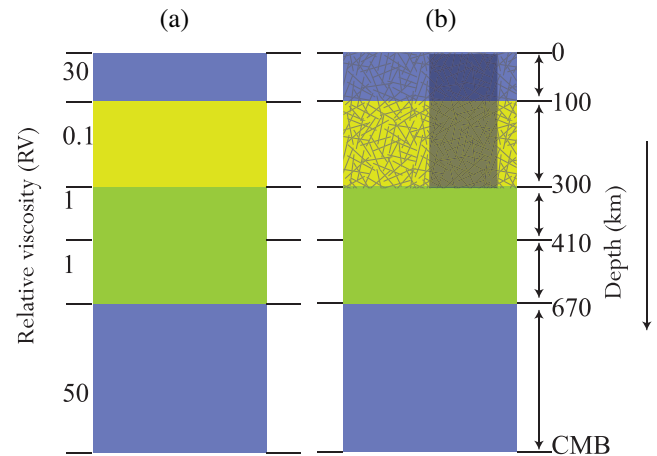


Figure 1. (a) Schematic diagram of the radial viscosity structure of the mantle that is considered in our model. Relative viscosity values with respect to a reference upper-mantle viscosity (10^{21} Pa-s) are marked on the left-hand side. (b) Temperature-dependent viscosity is introduced in the hatched area (up to 300 km). Additionally, highly viscous cratons (dark grey bar) are also incorporated.

used $65 \times 65 \times 65$ nodes per topological cap in CitcomS, which translates into average horizontal resolution of 0.7×0.7 degree. The vertical resolution is 24 km down to 300 km depth and 50 km below that. We impose free-slip boundary conditions at the surface and at the core–mantle boundary (CMB). In addition, we also simulate a few cases with a no-slip boundary condition at the surface in order to compare our results with those of Conrad & Lithgow-Bertelloni (2006). Density anomalies in the mantle are extracted from SMEAN2 tomography model [a composite model comprised of S40RTS (Ritsema *et al.* 2011), GyPSuM-S (Simmons *et al.* 2010) and SAVANI (Auer *et al.* 2014) using the methods of Becker & Boschi (2002)]. Sub-continental regions with positive seismic velocity anomaly shallower than 300 km are removed from the tomography model in order to impose neutrally buoyant cratons. A scaling ($d \ln \rho / d \ln V_s$) of 0.25 is used to convert seismic velocity anomaly to density anomaly (*cf.* Ghosh *et al.* 2017).

2.2 Mantle viscosity structure

We compare our results to a reference model with a radial viscosity structure, in which we have divided the mantle into five layers of different rheological strengths following Conrad & Lithgow-Bertelloni (2006; Fig. 1a). These layers are, respectively, lithosphere: 0–100 km; asthenosphere: 100–300 km; upper mantle: 300–410 km; transition zone: 410–670 km and lower mantle: 670 km CMB. The reference viscosity of the upper mantle (10^{21} Pa-s) is multiplied by relative viscosities in each of these layers, which are 30, 0.1, 1, 1 and 50, respectively. This makes the lithosphere and the lower mantle the strongest layers and the asthenosphere the weakest layer.

We develop models with LVV (Fig. 1b) in which high-viscosity cratons are introduced using the lithosphere thickness model of Conrad & Lithgow-Bertelloni (2006). Here, any lithosphere that is more than 180 km thick is considered cratonic. Lithosphere thickness in the range of 120–180 km is assumed to be intracratonic continental and is binned to 120 km in order to distinguish the cratonic regions. This assumption does not affect the result significantly as only ~ 7 per cent of the total area is between 120 and 180 km thick

(see contour lines in Fig. 2). For cratons, we assign a viscosity between the surface and the base of the craton that is a multiple of the reference viscosity structure. We run different models with different cratonic multiples between 10 and 1000 times the relative viscosities of each layer. Thus, a cratonic multiple of 100 means that the cratonic areas will have a net viscosity of 3×10^{24} Pa-s down to 100 km depth and 10^{22} Pa-s down to the base of the craton in case of asthenosphere viscosity of 10^{20} Pa-s. From the surface down to 300 km, we employ temperature-dependent viscosity using a linearized form of Arrhenius law, $\eta = \eta_0 \times \exp[E(T_0 - T)]$ (Frank-Kamenetskii 1969), where η_0 is the viscosity assigned for the ambient layer, for example, for top 100 km this is 30×10^{21} Pa-s. T_0 and T are non-dimensional reference and actual temperatures obtained by using a thermal expansivity of $3 \times 10^{-5} K^{-1}$ that converts density anomalies into temperature anomalies (*cf.* Ghosh *et al.* 2017). Because high-velocity anomalies are already removed under the cratons, their viscosity is not affected by temperature. Applying temperature dependence of viscosity to the entire mantle (instead of only above 300 km depth) yields nearly identical results. To apply the temperature-dependent viscosity, we have non-dimensionalized temperature with respect to 1300 °C mantle potential temperature. We have kept the background non-dimensionalized temperature as 0.5 and the non-dimensionalized temperature (T) varies between 0 and 1. E , a dimensionless number that determines the strength of the temperature dependence is kept as 5 (e.g. Ghosh *et al.* 2010), which translates to the weakest region having a viscosity ~ 10 times lower than the intraplate regions and which also gives rise to plate-like velocities (Fig. S1, Supporting Information). This set of assigned viscosity structures produce relatively low viscosity plate margins and comparatively higher viscosity intraplate regions (Fig. 2). We have tested a few models with E values greater than 5 (e.g. 10), but we find that these are unable to reproduce plate-like velocity patterns in the top 100 km. In particular, stronger temperature dependence of viscosity tends to stiffen colder plate boundary regions near subduction zones and prevents localized plate-like deformation there. Because asthenosphere viscosity is not very well constrained from experimental and numerical studies (e.g. Ghosh *et al.* 2008, 2013), we have tested different η_0 values for asthenosphere ranging from 10^{19} Pa-s (0.01 times the reference viscosity) to 10^{21} Pa-s (same as the reference viscosity) to produce nine different combinations of LVV models. These combinations lead to LVV that range from 10^{18} to 10^{25} Pa-s with a maximum variation of seven orders of magnitude.

2.3 Traction and strain-rate calculation

Viscous mantle flow exerts shear tractions at the base of lithosphere. We have extracted the $\tau_{r\phi}$ and $\tau_{r\theta}$ components (r , ϕ , and θ are the radial and lateral components in the polar coordinate system, where ϕ and θ are longitude and colatitude) of the total stress tensor at the lithospheric base (the depth of which varies laterally) and have calculated the resultant horizontal traction vectors. We compute shear strain-rates from the flow velocity of the finite element calculation by following the approach of Conrad *et al.* (2007), who ignored negligible horizontal gradients.

Using a no-slip boundary condition, we are able to reproduce the traction ratio calculated by Conrad & Lithgow-Bertelloni (2006; see their fig. 4 and the Supporting Information Fig. S2 of this paper), which was obtained by dividing the surface tractions in LVV models with the surface tractions in the reference (layered viscosity) model. In our case, using a free-slip boundary condition, we

have calculated tractions and strain-rates at the variable base of the lithosphere instead of at the surface. We have normalized strain-rates relative to their values at the same depth in the reference model. Normalizing the strain-rates thus represents the intensity of deformation associated with the LVV structure. Absolute values of tractions and normalized values of strain-rates are binned into nine intervals of ~ 24 km thickness from 0 to 270 km depth (bins in depth range from 120 to 180 does not have any contribution) and average values are further calculated from each bin interval.

3 TRACTION AT THE BASE OF THE LITHOSPHERE

Traction magnitudes (Fig. 3) increase under the highly viscous cratons with a few regions showing amplitudes as high as 13 MPa. Models with larger asthenosphere viscosity have significantly larger tractions than those with weaker asthenosphere. Away from the cratons, higher tractions are related to upper-mantle density anomalies (Fig. S3, Supporting Information). These include the subduction zones such as those in the Western Pacific and the Indian Ocean. A few parts of east Africa have high tractions because of velocity gradients associated with mantle upwelling at the East African Rift (Fig. S1, Supporting Information).

To look for sensitivity to viscosity structures, we have calculated the average traction magnitude at the variable base of the lithosphere. This average traction magnitude shows a dependence on asthenospheric viscosity, craton viscosity and lithosphere thickness (Fig. 4a). In particular, models with the weakest asthenosphere (0.01 times the reference viscosity) have the lowest average traction at the base of the lithosphere, and traction magnitude increases as the asthenosphere becomes stronger (Figs 3 and 4a). Viscosity and absolute traction roughly hold a linear relationship (with a correlation coefficient of 0.56, Fig. 4b), because stronger asthenosphere can more efficiently couple with the lithosphere, transmitting larger stresses. On the other hand, weaker asthenosphere promotes decoupling along the lithosphere–asthenosphere boundary that hinders stress transmission, resulting in a lowering of average traction magnitude. For the same reason, tractions are larger beneath more highly viscous cratons (Fig. 4a).

We also find that traction magnitudes tend to increase with lithosphere thickness (Fig. 4a). This increase is primarily controlled by the free-slip boundary condition imposed at the surface. Under such conditions, shear tractions become zero at the surface and gradually increase with depth. Beneath the thinnest lithosphere, that is, mid-oceanic ridges, average traction magnitude is only a fraction of a megapascal. This average traction magnitude increases with lithosphere thickness until 100 km, although below continental lithosphere (96–120 km thick), traction values do not change significantly. Under thick cratons, tractions also increase with lithosphere thickness, and the maximum value of traction magnitude occurs around 216 km, which is the depth that corresponds to most craton edges (Fig. 4a). At depths greater than 216 km, traction magnitudes drop again. We speculate that this might be because of high stresses getting absorbed at the edges of cratons with the cratonic cores being less stressed. Traction beneath cratonic regions are several times larger than those for the reference model (the black dashed line in Fig. 4a), which does not have cratons. Our finding that tractions increase with lithospheric thickness is similar to what Conrad & Lithgow-Bertelloni (2006) found for flow calculations beneath a rigid lid.

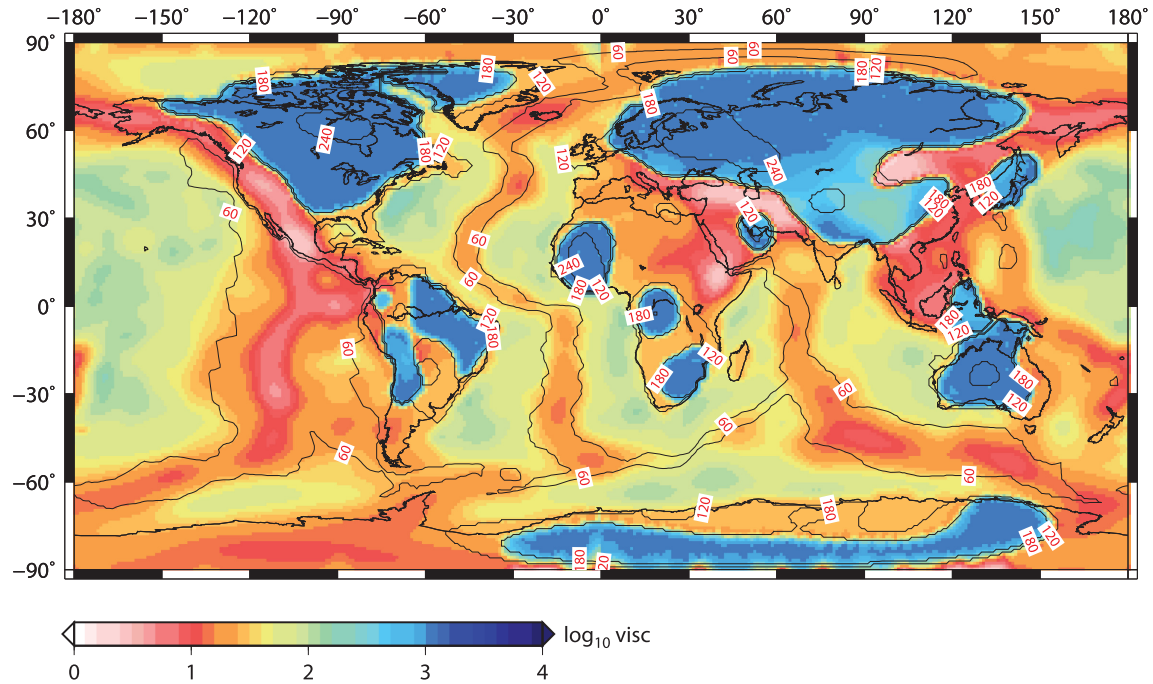


Figure 2. Laterally varying viscosity map at 24 km depth from a model with 100 times viscosity contrast between cratons and the surrounding layer. The background colour represents normalized value of LVV with respect to the reference viscosity of upper mantle (10^{21} Pa-s). In the model, actual viscosity ranges from 10^{19} to 10^{24} Pa-s. Since the representative viscosity is plotted within the lithosphere, the viscosity ranges only between 10^{21} and 10^{24} Pa-s. However, within asthenosphere (~ 100 – 300 km depth) viscosity drops to $\sim 10^{19}$ Pa-s. Lithospheric thickness is obtained from the model of Conrad & Lithgow-Bertelloni (2006) and is represented by black contour lines. Lithosphere greater than 180 km thick is considered as cratonic in our model.

4 STRAIN-RATES AT THE BASE OF THE LITHOSPHERE

We similarly compute maps of normalized strain-rates (Fig. 5), which are strain-rates at the base of lithosphere in LVV models divided by the strain-rate at same depth in reference radial model. Strain-rates at the base of the lithosphere should ideally scale with shear tractions: the larger tractions associated with greater asthenosphere viscosity will tend to produce larger strain-rates. However, we observe the opposite behaviour beneath cratons, where stiffer asthenosphere (or stronger cratons) leads to smaller strain-rates (Figs 5 and 6a). Additionally, we observe notably diminished strain-rate magnitudes (slowest deformation rates) under the cratons (Fig. 5), which is the opposite of what we found for tractions. Indeed, we note that average strain-rates drop monotonically with lithosphere thickness (Fig. 6) for stronger asthenosphere (10^{20} and 10^{21} Pa-s), despite an opposing trend of increasing tractions (Fig. 4a). Models with an asthenospheric viscosity of 10^{19} Pa-s (0.01 times reference viscosity) show a jump at around 120 km depth beyond which strain-rates decrease similarly as the other models. At the core of cratons, where lithosphere thickness is largest, the normalized strain-rates are minimum. This indicates that cratonic cores suffer much less deformation compared to any other part of the lithosphere.

5 DISCUSSION

5.1 Traction and strain-rate relation

Our calculations show that traction magnitudes at the base of the lithosphere are governed by three main factors: viscosity of asthenosphere, viscosity of cratons and lithospheric thickness. We find that

even though tractions are largest beneath cratons, deformation at their base is slow. Indeed, tractions and strain-rates at the base of the lithosphere are inversely related (Fig. 6b), which may not be intuitive. This sort of relationship is only possible if the ‘apparent viscosity’ of the lithosphere depends strongly on thickness. Here we consider that apparent viscosity represents an average viscosity for the lithosphere that can resist shear deformation across the lithospheric thickness. To estimate an apparent viscosity, we assume an average horizontal velocity drop across the lithosphere’s thickness (from the top of the lithosphere to the base of the lithosphere). Dividing this average velocity drop (δv) by the thickness of the lithosphere (h) gives an estimate of the average lithospheric strain-rate. The apparent viscosity (η_{ap}) that is responsible for deformation at the base of the lithosphere can then be obtained by dividing absolute traction (σ_t) by the average lithospheric strain-rate:

$$\eta_{ap} = \frac{\sigma_t}{\delta v/h}, \quad (1)$$

where η_{ap} can be scaled to h^2 assuming δv is constant and σ_t varies linearly with h . Hence, the apparent viscosity, $\eta_{ap} \sim h^2$. We see that in the reference case (marked by black dashed line in Fig. 7a) η_{ap} does not show much variation with thickness. Introducing LVV changes the strength of the lithosphere and thus results in different apparent viscosity, as shown by the varying slopes in the relation between η_{ap} and h^2 .

The apparent viscosity plotted against the square of the thickness of the lithosphere shows a positive and modest linear relationship (Fig. 7a). This means that as the lithosphere becomes thicker, it can resist more deformation. So, introducing a free-slip condition results in increased traction magnitude and the laterally varying viscosity structure results in decreasing strain-rates for

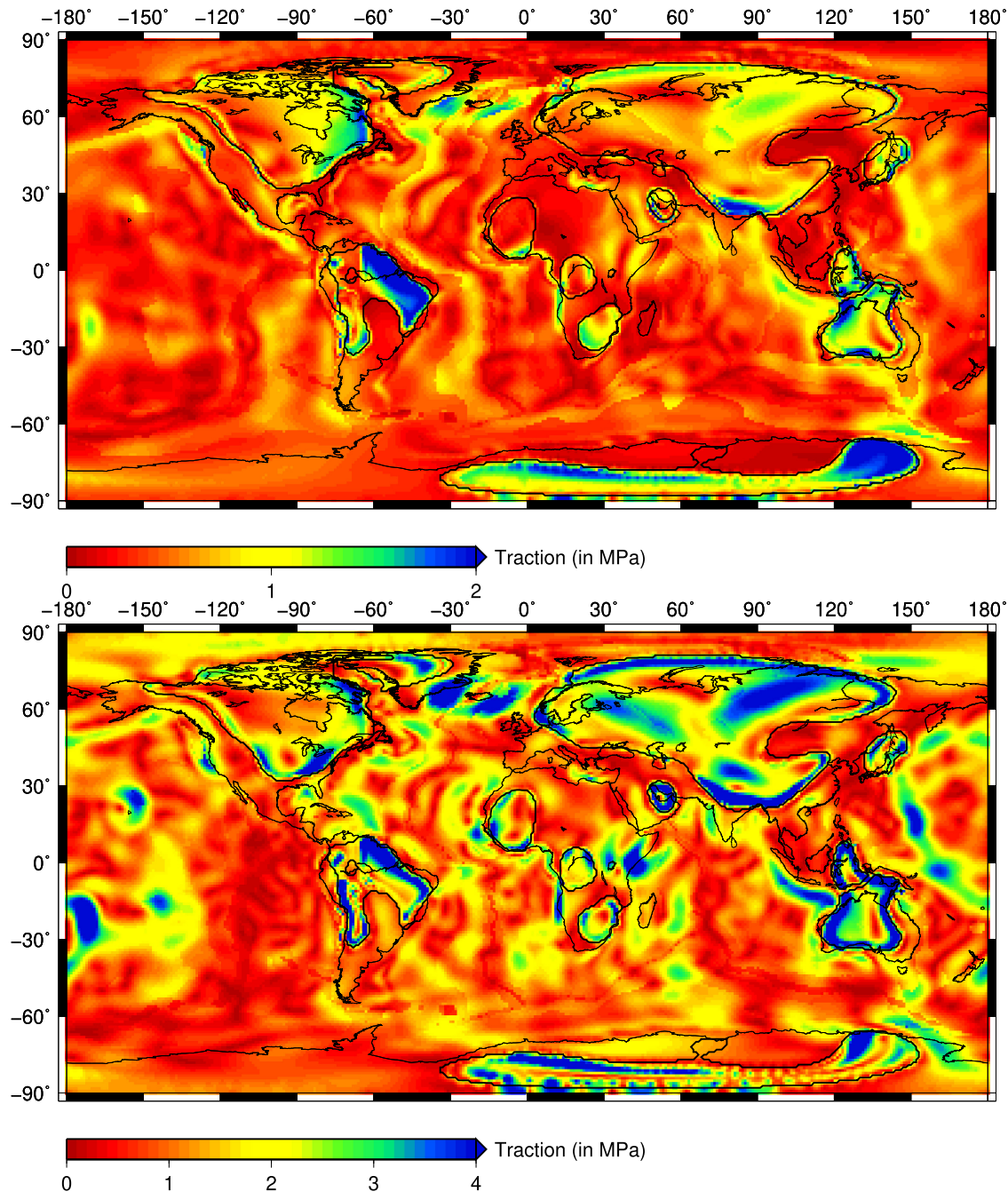


Figure 3. Map view of the traction magnitudes at the variable base of the lithosphere. Two figures show results from two models with different asthenosphere viscosity of 10^{19} Pa-s (0.01 times reference viscosity) (Top) and 10^{21} Pa-s (same as reference viscosity) (Bottom), both with 100 times viscosity contrast for cratons. Magnitudes greater than 2 MPa (for top figure) and 4 MPa (for bottom figure) are saturated in the blue colour. Craton boundaries are marked by the thick black lines.

thicker lithosphere. The combination of these two effects results in an inverse relation between traction and strain-rate. Cooper & Conrad (2009) did not consider weak plate boundaries and thus tractions exerted on the lithospheric base accumulated under thick cratons, resulting in significant local shearing of the lithosphere. By contrast, because of our LVV implementation strain can accumulate along the weak lithospheric margins (e.g. plate boundaries) leaving plate interiors relatively unaffected. Thicker cratons, with higher apparent viscosity, are thus the least deformed parts of the lithosphere.

5.2 Survival of cratons over ages

In this section, we attempt to find a relation between the survival time of cratons and that of the oceanic lithosphere by using their associated strain-rates. We assume that lithosphere gets destroyed by accumulating strain with time. So, slower strain-rates applied to the lithosphere should allow it to survive longer. Hence, we can approximate the survival time of lithosphere as inversely proportional to the strain-rate. Let us consider t_{cd} and t_{od} as the survival duration of cratonic and oceanic lithosphere, respectively, and let T_c be their ratio ($T_c = t_{cd}/t_{od}$). The average survival time of oceanic lithosphere

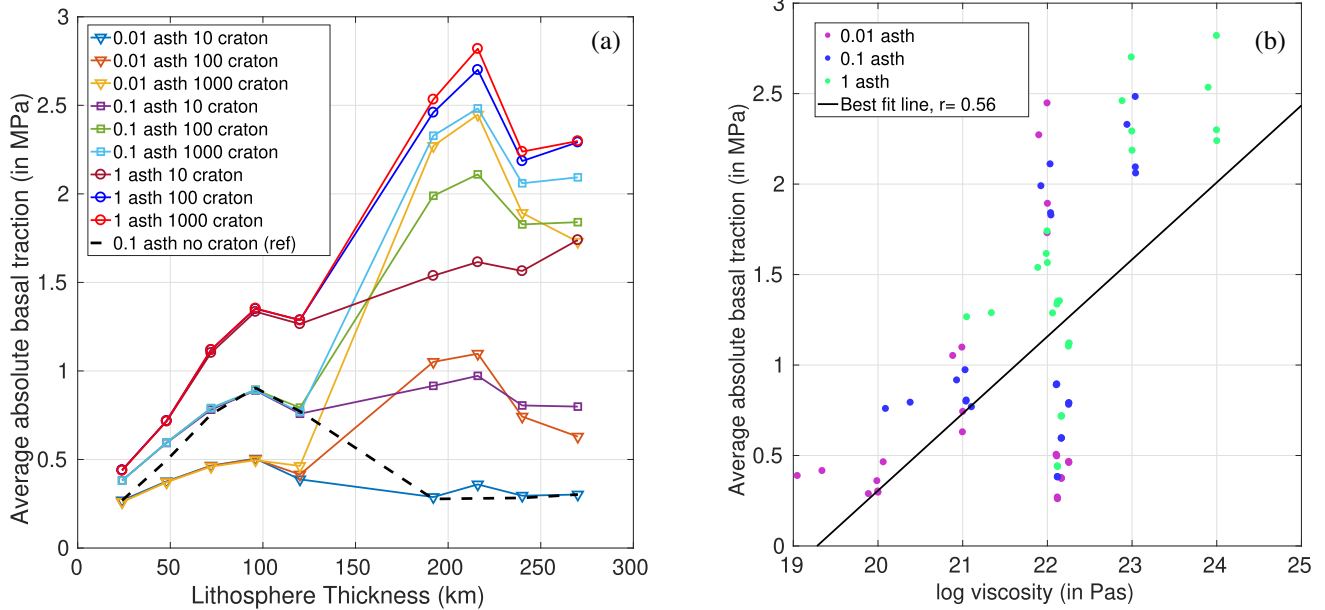


Figure 4. (a) Variation of average absolute traction magnitude at the base of the lithosphere. Each line of different symbol and colour represents the magnitude of absolute traction obtained from a model of certain viscosity combinations as presented in the legend. Viscosity of the asthenosphere is with respect to the reference viscosity (10^{21} Pa-s). The dotted black line is the result obtained from the reference radial model. (b) The relation between average absolute traction magnitude and asthenospheric viscosity. The coloured dots represent different η_0 of the asthenosphere. The black line is the best-fitted line for traction magnitude and asthenospheric viscosity with a correlation of 0.56.

on the Earth is around 180 Ma (Stern & Scholl 2010), although the mechanism of destruction of oceanic lithosphere is subduction, which is not the same as that for cratons. Hence, we take a range of t_{od} between 80 Ma, which is the time at which the ocean floor starts to flatten because of convective instability (Davaille & Jaupart 1994; Huang *et al.* 2003), and 180 Ma, when most of the ocean floor gets destroyed by subduction. We take the average normalized strain-rates under the cratons (>200 km thick, $\dot{\epsilon}_c$) and the oceanic lithosphere (0–72 km thick, $\dot{\epsilon}_o$). The ratio ($\dot{\epsilon}_o / \dot{\epsilon}_c$), which we call inverse of non-dimensionalized strain-rates (INS), scales with T_c .

$$T_c = \frac{t_{cd}}{t_{od}} \equiv 1 / \left(\frac{\dot{\epsilon}_c}{\dot{\epsilon}_o} \right) = \text{INS}. \quad (2)$$

Thus, if a craton has to survive n times the age of an oceanic lithosphere, it must experience strain-rates that are at least $1/n$ times those appropriate for the oceanic lithosphere. This non-dimensionalization indicates how fast oceanic lithosphere can be destroyed compared to a craton.

If the inverse of non-dimensionalized strain-rate (INS) of a craton is greater than the ratio of survival time (T_c) of a particular age (Table 1), then that craton can potentially survive longer than that age. We compare this range to the endurance of a craton existing since the Cambrian (540 Ma) and obtain $T_{cmax} = 6.8$ for t_{od} of 80 Ma, and $T_{cmin} = 3$ for $t_{od} = 180$ Ma. If a craton is stable since Cambrian, its INS value should be within or more than the [3–6.8] range. Survival time ratios for longer cratonic ages of Proterozoic, 3 Ga (peak craton stabilization time) and Archean are even greater (Table 1).

We compute the INS values for our models (Fig. 7b) and find that the model with weakest asthenosphere and weakest cratons (0.01, 10) has $\text{INS} = 1.3$, which is smaller than T_c for Cambrian (Table 1). Thus, for this viscosity combination, cratonic lithosphere formed in Cambrian will not be able to survive to the present day. Cratons of 100 times viscosity contrast (0.01, 100) have $\text{INS} = 3.1$ that

falls within the T_c range for the Cambrian. 1000 times viscosity contrast cratons (0.01, 1000) have INS value (10.4) greater than the Cambrian T_c range, and thus may potentially be stable beyond the Cambrian. The combination of a moderately viscous asthenosphere (10^{20} Pa-s) and cratons of 100 times viscosity contrast (0.1, 100; $\text{INS} = 14.2$) can also potentially be stable beyond the Cambrian. Within the same moderately viscous asthenosphere, a craton of 1000 times viscosity contrast (0.1, 1000; $\text{INS} = 64.1$) formed during the Archean can survive until today. If the asthenosphere viscosity is kept at 10^{21} Pa-s (same as upper-mantle viscosity), cratons of 100 times viscosity contrast (1, 100; $\text{INS} = 51.3$) may stabilize even beyond the Archean, and more viscous cratons could potentially survive for a much longer time.

We have examined a wide interval of t_{cd} values, yet the scaling of strain-rates shows a consistent pattern of viscosity combinations that are required for cratonic survival for different timescales. In particular, models with an asthenospheric viscosity that is 100 times smaller than that of the upper mantle will generally not allow cratons to survive beyond Archean, but asthenospheric viscosity contrasts of 10 or smaller will permit this. According to a study by Gung *et al.* (2003), a low-viscosity channel beneath the cratons satisfies some seismic constraints but our results suggest that such a layer should not have a viscosity lower than $\sim 10^{20}$ Pa-s. We note that our estimate of the viscosity combination for a given craton and asthenosphere is a minimum requirement for a craton to survive for a certain period of time, provided that basal traction is the only destructive force acting to destabilize cratons. We do not consider the delamination of cratons due to gravitational instability. Other destructive mechanisms (e.g. viscous drainage, rheological weakening; see Lee *et al.* 2011 for details) will additionally affect the long-term survival of cratons. This exercise of interpreting INS values in terms of the long-term survival potential of cratons has the additional limitation that oceanic lithosphere and cratons do not get destroyed by the same tectonic process, and thus the reference age

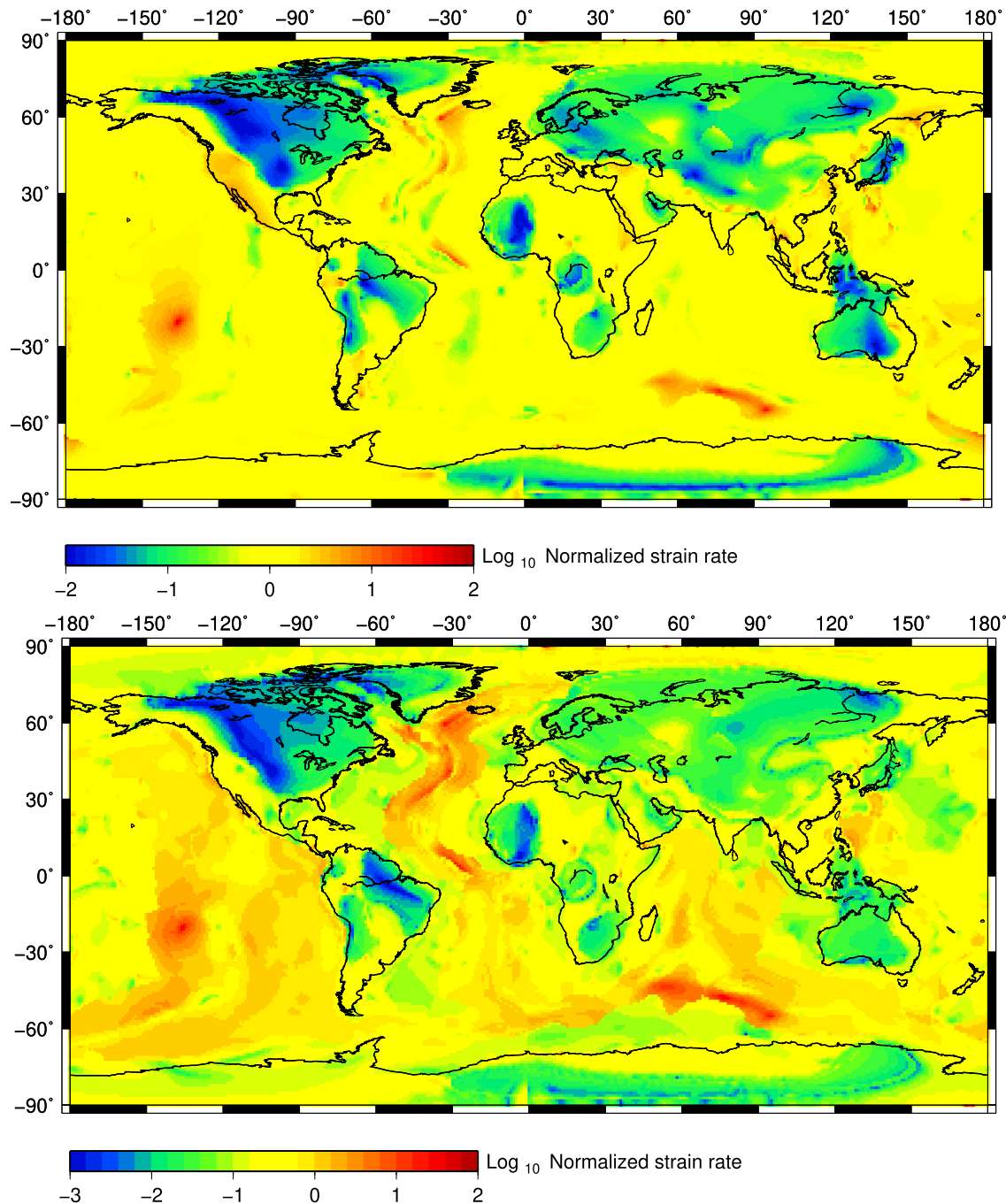


Figure 5. Map view of the normalized strain-rate magnitudes at the variable base of the lithosphere. Two figures show the result from two models with different asthenosphere viscosity of 10^{20} Pa-s (Top) and 10^{21} Pa-s (Bottom). In both the cases, viscosity contrast of craton is 100.

for oceanic destruction is rather uncertain. We have also calculated rates of lithospheric thickness changes associated with thermal cooling. We find (Fig. S4, Supporting Information) that thermal cooling tends to change lithospheric thickness more slowly than deformation due to mantle shearing. As thermal cooling is slower than deformation, it is unlikely to significantly impact cratonic survival. But if it did have any influence, it would be to further stabilize the cratons. Thus our estimates represent a lower bound to the stable ages of cratons of different viscosities. We also show that the thickness of the cratons may help to explain their longevity compared

to non-cratonic continental areas, which tend to have lithosphere that is both thinner and younger than cratons (Poupinet & Shapiro 2009).

To understand the complete scenario of cratonic survival, time-dependent geodynamic models may be required. Because we use instantaneous models, we have extrapolated the strain-rates linearly in time to gauge long-term stability or instability of cratons. A time-dependent study, which is more challenging in terms of data scarcity for the early earth and computational expenses, can, however, address gravitational dripping and changes to strain-rates with time.

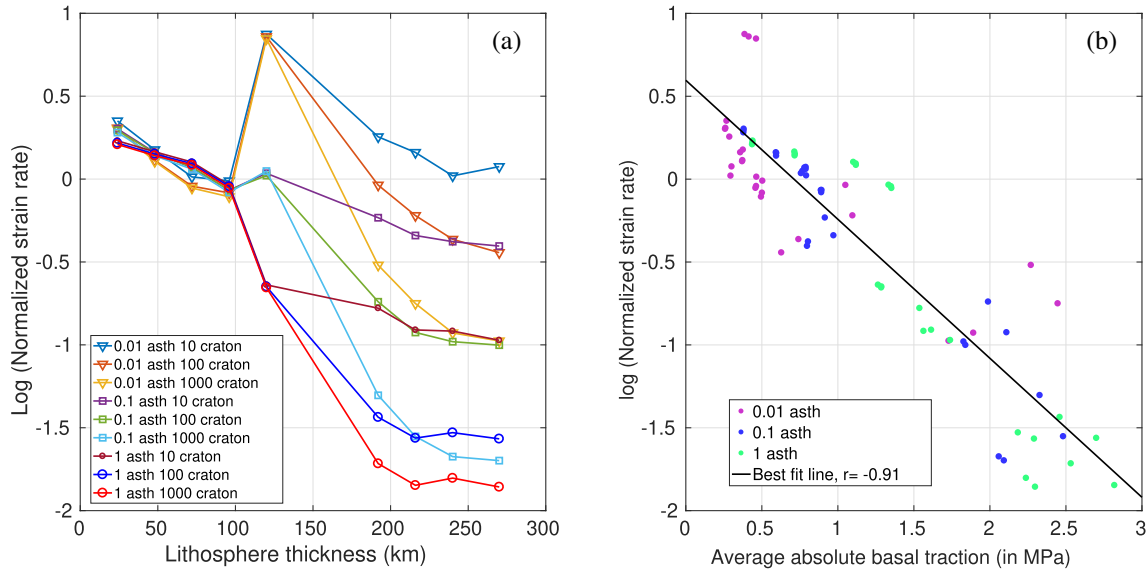


Figure 6. (a) Variation of average normalized strain-rate at the base of the lithosphere. Each line of different symbol and colour represents the magnitude of the normalized strain-rate obtained from a model with a certain viscosity combination as presented in the legend. (b) The relation between traction and normalized strain-rates at the base of the lithosphere. The different coloured dots represent different viscosities of asthenosphere with respect to the upper-mantle viscosity.

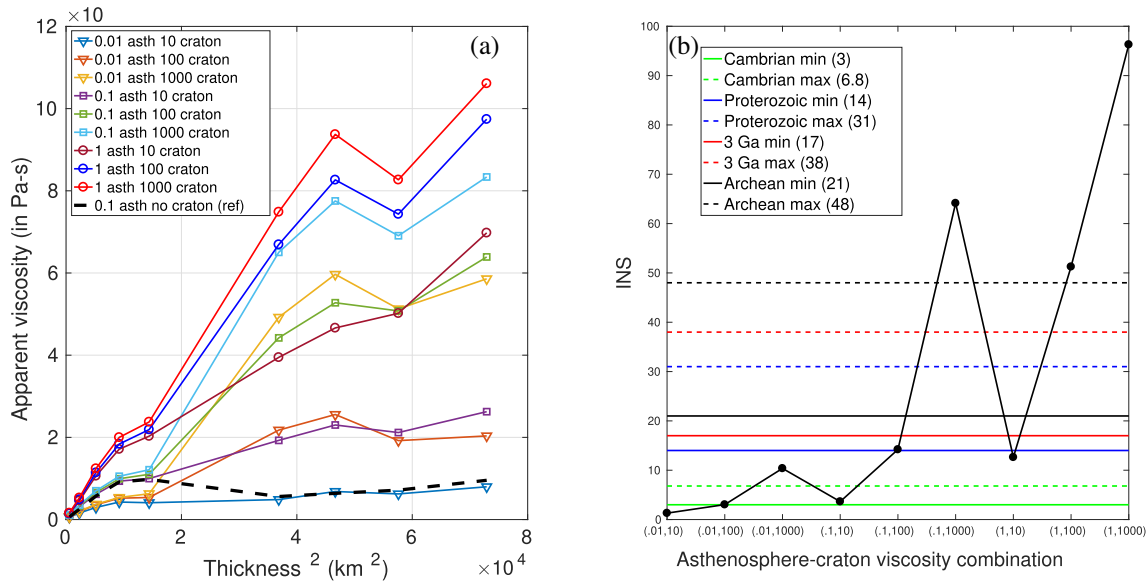


Figure 7. (a) Apparent viscosity plotted against the square of the lithosphere thickness from different models. Each line of different symbol and colour represents a model with a certain viscosity combination similar to Fig. 4(a). (b) Analysis of cratonic survival time. In the x-axis, the first number within each pair of parentheses denotes asthenosphere viscosity with respect to upper-mantle viscosity and the second number denotes craton viscosity contrast. The coloured horizontal lines indicate T_c for Cambrian, Proterozoic, Archean and at 3 Ga γ -axis indicates INS values.

Table 1. Calculation of T_c for different geological ages.

Geological time	t_{cd} (in Ma)	T_{cmin} for 180 Ma	T_{cmax} for 80 Ma
Cambrian	540	3	6.8
Proterozoic	2500	14	31
Peak craton stabilization	3000	17	38
Archean	3850	21	48

Also, in this study, we have considered Newtonian rheology under the cratons while some studies (Cooper & Conrad 2009; Wang *et al.* 2014) have suggested that cratons might deform according to non-Newtonian flow laws.

6 CONCLUSION

To understand the nature of convective shearing at the base of the lithosphere, we have used free-slip boundary conditions at the surface of instantaneous global mantle flow models while imposing LVV, which have allowed stresses to accumulate along weak plate boundaries. We infer that tractions at the base of the lithosphere are dependent on the viscosity of asthenosphere, the viscosity of cratons and the thickness of lithosphere. Cratons, being highly viscous, have maximum traction magnitudes at their base. However, despite being highly stressed regions, we find that these cratons are the slowest deforming areas. Such slow deformation enhances their survival over geological time. We found an inverse relationship

between stress and strain-rate at the base of the lithosphere, which we attribute to an increase in the apparent viscosity of the lithosphere with the square of the lithosphere thickness. Clearly, in our models with LVV, thick cratons become more difficult to deform than the oceanic lithosphere and the thinner continental regions that surround the cratons. As thicker cratons have higher apparent viscosity, higher traction values at their base cause the lithosphere to move laterally rather than to deform locally. This leads to strain localization along weak zones (e.g. plate boundaries). Hence, cratons remain as the least deformed regions, despite having higher tractions beneath them.

By examining different viscosity combinations for cratons and asthenosphere, we have also evaluated the impact of viscosity on the long-term survival potential of cratons. Although time-dependent models would significantly augment this study, our calculations from instantaneous models can also shed light on the factors that control continental survival timescales. We find that greater viscosities for either the asthenosphere or the cratons (or both) tend to promote long-term survival, as does enhanced craton thickness. Why cratons have survived over such long periods of time is still an unsolved problem, with potentially many various factors exerting important controls on a variety of deformation mechanisms. We identify the slow deformation at the base of cratons, which we have shown to be associated with their thickness and viscosity, to be one key factor that has helped to ensure cratonic survival over geologic time.

ACKNOWLEDGEMENTS

We thank three anonymous reviewers for their valuable input that improved the manuscript. Convection code CitcomS-3.3.1 is maintained by Computational Infrastructure for Geodynamics (CIG). The work was carried out at the Computational Geodynamics lab at CEAs, IISc and all models were run using a Cray XC40 system at the Supercomputer Education and Research Centre (SERC), IISc. Figures were produced using GMT 4.5.11 by P. Wessel and W. F. Smith and MATLAB 9.1 licensed at IISc. JP was funded by the Institute (IISc) scholarship. This work was partly supported by the Research Council of Norway through its Centres of Excellence funding scheme, project number 223272.

REFERENCES

- Artemieva, I. & Mooney, W., 2002. On the relations between cratonic lithosphere thickness, plate motions, and basal drag, *Tectonophysics*, **358**(1), 211–231.
- Auer, L., Boschi, L., Becker, T., Nissen-Meyer, T. & Giardini, D., 2014. Savani: a variable resolution whole-mantle model of anisotropic shear velocity variations based on multiple data sets, *J. geophys. Res.*, **119**(4), 3006–3034.
- Beall, A., Moresi, L. & Cooper, C., 2018. Formation of cratonic lithosphere during the initiation of plate tectonics, *Geology*, **46**(6), 487–490.
- Becker, T. & Boschi, L., 2002. A comparison of tomographic and geodynamic mantle models, *Geochem. Geophys. Geosyst.*, **3**(1), doi:10.1029/2001GC000168.
- Conrad, C., Behn, M. & Silver, P., 2007. Global mantle flow and the development of seismic anisotropy: differences between the oceanic and continental upper mantle, *J. geophys. Res.*, **112**(B7), doi:10.1029/2006JB004608.
- Conrad, C.P. & Lithgow-Bertelloni, C., 2006. Influence of continental roots and asthenosphere on plate-mantle coupling, *Geophys. Res. Lett.*, **33**(L05), 312, doi:10.1029/2005GL025621.
- Cooper, C. & Conrad, C.P., 2009. Does the mantle control the maximum thickness of cratons? *Lithosphere*, **1**(2), 67–72.
- Cooper, C., Lenardic, A., Levander, A. & Moresi, L.N., 2006. Creation and preservation of cratonic lithosphere: seismic constraints and geodynamic models, in *Archean Geodynamics and Environments*, pp. 75–88, eds, Benn, K., Condie, J.M. & American, K.C., Geophysical Union.
- Davaille, A. & Jaupart, C., 1994. Onset of thermal convection in fluids with temperature-dependent viscosity: application to the oceanic mantle, *J. geophys. Res.*, **99**(B10), 19 853–19 866.
- Frank-Kamenetskii, D.A., 1969. *Diffusion and Heat Transfer in Chemical Kinetics*, Plenum Press.
- Ghosh, A., Holt, W., Wen, L., Haines, A. & Flesch, L., 2008. Joint modeling of lithosphere and mantle dynamics elucidating lithosphere-mantle coupling, *Geophys. Res. Lett.*, **35**(16), doi:10.1029/2008GL034365.
- Ghosh, A., Becker, T. & Zhong, S., 2010. Effects of lateral viscosity variations on the geoid, *Geophys. Res. Lett.*, **37**(1), doi:10.1029/2009GL040426.
- Ghosh, A., Holt, W. & Wen, L., 2013. Predicting the lithospheric stress field and plate motions by joint modeling of lithosphere and mantle dynamics, *J. geophys. Res.*, **118**(1), 346–368.
- Ghosh, A., Thyagarajulu, G. & Steinberger, B., 2017. The importance of upper mantle heterogeneity in generating the Indian Ocean geoid low, *Geophys. Res. Lett.*, **44**(19), 9707–9715.
- Gung, Y., Panning, M. & Romanowicz, B., 2003. Global anisotropy and the thickness of continents, *Nature*, **422**(6933), 707–711.
- Hawkesworth, C., Cawood, P.A. & Dhuime, B., 2016. Tectonics and crustal evolution, *GSA Today*, **26**(9), 4–7.
- Hawkesworth, C., Cawood, P.A., Dhuime, B. & Kemp, T.I., 2017. Earth's continental lithosphere through time, *Annu. Rev. Earth Planet. Sci.*, **45**(1), 169–198.
- Huang, J., Zhong, S. & van Hunen, J., 2003. Controls on sub-lithospheric small-scale convection, *J. geophys. Res.*, **108**(B8), doi:10.1029/2003JB002456.
- Jordan, T., 1975. The continental tectosphere, *Rev. Geophys.*, **13**(3), 1–12.
- Jordan, T., 1978. Composition and development of the continental tectosphere, *Nature*, **274**(5671), 544–548.
- Kaban, M., Mooney, W. & Petrunin, A., 2015. Cratonic root beneath North America shifted by basal drag from the convecting mantle, *Nat. Geosci.*, **8**(10), 797–800.
- King, S., 2005. Archean cratons and mantle dynamics, *Earth planet. Sci. Lett.*, **234**(1), 1–14.
- Lee, C.-T.A., Luffi, P. & Chin, E.J., 2011. Building and destroying continental mantle, *Annu. Rev. Earth Planet. Sci.*, **39**, 59–90.
- Lenardic, A. & Moresi, L.N., 1999. Some thoughts on the stability of cratonic lithosphere: effects of buoyancy and viscosity, *J. geophys. Res.*, **104**(B6), 12 747–12 758.
- Lenardic, A., Moresi, L.N. & Mühlhaus, H., 2000. The role of mobile belts for the longevity of deep cratonic lithosphere: the crumple zone model, *Geophys. Res. Lett.*, **27**(8), 1235–1238.
- Lenardic, A., Moresi, L.N. & Mühlhaus, H., 2003. Longevity and stability of cratonic lithosphere: insights from numerical simulations of coupled mantle convection and continental tectonics, *J. geophys. Res.*, **108**(B6), doi:10.1029/2002JB001859.
- Moore, W.B. & Webb, A.A.G., 2013. Heat-pipe earth, *Nature*, **501**(7468), 501–505.
- O'Neill, C., Lenardic, A., Griffin, W. & O'Reilly, S., 2008. Dynamics of cratons in an evolving mantle, *Lithos*, **102**(1), 12–24.
- Pearson, D. & Wittig, N., 2014. The formation and evolution of cratonic mantle lithosphere—evidence from mantle xenoliths, in *Treatise on Geochemistry*, pp. 255–292, eds, Turekian, K. & Holland, H., Elsevier.
- Pearson, D., Carlson, R., Shirey, S., Boyd, F. & Nixon, P., 1995a. Stabilisation of Archaean lithospheric mantle: a Re-Os isotope study of peridotite xenoliths from the Kaapvaal craton, *Earth planet. Sci. Lett.*, **134**(3), 341–357.
- Pearson, D., Snyder, G., Shirey, S., Taylor, L. *et al.*, 1995b. Archaean Re-Os age for Siberian eclogites and constraints on Archaean tectonics, *Nature*, **374**(6524), 711–713.
- Polet, J. & Anderson, D., 1995. Depth extent of cratons as inferred from tomographic studies, *Geology*, **23**(3), 205–208.

- Poupinet, G. & Shapiro, N., 2009. Worldwide distribution of ages of the continental lithosphere derived from a global seismic tomographic model, *Lithos*, **109**(1-2), 125–130.
- Ritsema, J., Deuss, A.A., Van Heijst, H. & Woodhouse, J., 2011. S40rts: a degree-40 shear-velocity model for the mantle from new Rayleigh wave dispersion, teleseismic traveltimes and normal-mode splitting function measurements, *Geophys. J. Int.*, **184**(3), 1223–1236.
- Rudnick, R., McDonough, W. & O'Connell, R., 1998. Thermal structure, thickness and composition of continental lithosphere, *Chem. Geol.*, **145**(3), 395–411.
- Shapiro, S., Hager, B. & Jordan, T., 1999. Stability and dynamics of the continental tectosphere, *Lithos*, **48**(1), 115–133.
- Simmons, N.A., Forte, A.M., Boschi, L. & Grand, S.P., 2010. Gypsum: a joint tomographic model of mantle density and seismic wave speeds, *J. geophys. Res.*, **115**, doi:10.1029/2010JB007631.
- Sizova, E., Gerya, T., Stüwe, K. & Brown, M., 2015. Generation of felsic crust in the Archean: a geodynamic modeling perspective, *Precambrian Res.*, **271**, 198–224.
- Sleep, N.H., 2003. Survival of archean cratonic lithosphere, *J. geophys. Res.*, **108**(B6), doi:10.1029/2001JB000169.
- Stern, R.J. & Scholl, D.W., 2010. Yin and yang of continental crust creation and destruction by plate tectonic processes, *Int. Geol. Rev.*, **52**(1), 1–31.
- Tang, M., Chen, K. & Rudnick, R.L., 2016. Archean upper crust transition from mafic to felsic marks the onset of plate tectonics, *Science*, **351**(6271), 372–375.
- Wang, H., van Hunen, J., Pearson, D.G. & Allen, M.B., 2014. Craton stability and longevity: the roles of composition-dependent rheology and buoyancy, *Earth planet. Sci. Lett.*, **391**, 224–233.
- Yoshida, M., 2010. Preliminary three-dimensional model of mantle convection with deformable, mobile continental lithosphere, *Earth planet. Sci. Lett.*, **295**(1), 205–218.
- Yoshida, M., 2012. Dynamic role of the rheological contrast between cratonic and oceanic lithospheres in the longevity of cratonic lithosphere: a three-dimensional numerical study, *Tectonophysics*, **532**, 156–166.
- Zhong, S., Zuber, M., Moresi, L.N. & Gurnis, M., 2000. Role of temperature-dependent viscosity and surface plates in spherical shell models of mantle convection, *J. geophys. Res.*, **105**(B5), 11 063–11 082.

SUPPORTING INFORMATION

Supplementary data are available at *GJI* online.

Figure S1. Velocity vectors are plotted above viscosity structure at 24 km depth from models with a viscosity combination of 10^{20} Pa-s asthenosphere and cratons of 100 times viscosity contrast. Background colour represents normalized value of LVV with respect to the reference viscosity of upper mantle.

Figure S2. Traction ratio calculated at the surface from models using no-slip boundary conditions (similar to Conrad & Lithgow-Bertelloni 2006). Lines of different colours are obtained from models of different viscosity combinations of asthenosphere and cratons mentioned in the legend.

Figure S3. Top: Traction magnitudes at the base of the lithosphere from a model without any density anomaly in the upper mantle (till 670 km) but with LVV arising from high-viscosity cratons (100 times more viscous than intraplate areas). In this case, higher tractions are found to occur only underneath the cratons. Bottom: Traction magnitudes at the base of the lithosphere from a model with no LVV but with density anomalies in the entire mantle. High tractions occur under the plate margins (the Pacific, the Indian Ocean and the East African rift). Cratons do not show high tractions in this case.

Figure S4. We calculate lithospheric thickening rates due to thermal cooling. If we take thermal cooling timescale as $\tau = \frac{l^2}{\kappa}$, where l is the lithospheric thickness in the order of kilometres and κ is the thermal diffusivity in m^2/s , then, lithospheric thickening rate scales with $\dot{\epsilon}_c \sim \frac{1}{\tau}$. Hence, the normalized rate (q') becomes $q' = \frac{\dot{\epsilon}_c}{\dot{\epsilon}_0} = \frac{1}{\tau \times \dot{\epsilon}_0}$, where $\dot{\epsilon}_0$ is the average strain-rate at the base of 120 km thick lithosphere. This normalization indicates the intensity of lithospheric thickening due to thermal cooling compared to mantle shearing at the base of 120 km thick lithosphere. The result (black dashed line) shows that the thickening rate due to cooling is much slower than the deformation rate due to mantle shearing.

Please note: Oxford University Press is not responsible for the content or functionality of any supporting materials supplied by the authors. Any queries (other than missing material) should be directed to the corresponding author for the paper.